RSC Applied Interfaces

PAPER

View Article Online
View Journal | View Issue

Cite this: *RSC Appl. Interfaces*, 2024, 1, 245

A fluorinated perylene diimide for polar and non-polar green solvent processed organic photovoltaic cathode interlayers†

Colton Atkinson, Muhammad Rizwan Niazi and Gregory C. Welch *

Cathode interlayer materials (CILs) for solution-processed organic photovoltaics (OPVs) serve an instrumental role in mitigating charge extraction challenges to achieve high power conversion efficiencies (PCEs). Critical to the mass commercialization of OPV technologies is the use of green solvents to process the multi-layer devices (including the CIL) *via* roll-to-roll (R2R) compatible coating methods. To address this we report on a new fluorinated N-annulated 2-ethylhexyl substituted perylene diimide material (F-PDIN-EH) and its use as a CIL in conventional OPV devices processable from non-halogenated and non-aromatic solvents. Solubility measurements reveal enhanced processability from green solvents such as ethyl acetate, 1-butanol, and *n*-heptane for F-PDIN-EH as compared to non-fluorinated reference compound PDIN-EH. OPVs fabricated under ambient conditions using F-PDIN-EH as the CIL processed from polar solvents butanol and ethyl acetate or the non-polar solvent heptane exhibit similar PCEs of 10%. This is the first report of heptane, a non-polar and moderately green solvent, being used to process a CIL, and thus we further exploited this result and demonstrated the scalable processing of F-PDIN-EH using the roll-to-roll compatible slot-die coating method. OPV devices with slot-die-coated F-PDIN-EH films exhibited performance metrics on par with lab-scale spin-coated devices of the same architecture demonstrating industrial application.

Received 8th September 2023,
Accepted 15th October 2023

DOI: 10.1039/d3lf00166k

rsc.li/RSCApplInter

Introduction

Solution processed organic photovoltaics (OPVs) have garnered much interest owing to a compatibility with low-cost roll-to-roll (R2R) manufacturing methods and use in power applications under both artificial light and sunlight.[1–3] The high level of interest in the field has resulted in the development of novel photoactive materials, most notably non-fullerene acceptors, such as Y6, as well as the advancement of thin-film printing technologies and device engineering which combined have now brought lab-scale OPV power conversion efficiencies (PCEs) to greater than 19%.[4–7]

In conventional OPV devices an interfacial cathode interlayer (CIL) responsible for the efficient extraction of electrons from the active layer is crucial to realizing these high PCE metrics.[8–10] The improved efficiency of charge extraction is enabled by the CILs ability to tune the cathodic work function, reducing the energetic barrier between the metal electrode and organic bulk heterojunction (BHJ).[9,11] Conjugated polymers, metal oxides, and organic molecules are proven materials to be used as CILs in high performance OPVs.[12–14] However, metal oxide based CILs often react with BHJ materials leading to unstable OPVs.[15] While polymer type CILs face challenges in purification, complex syntheses, and limited batch-to-batch reproducibility, limiting their viability for commercial OPV technologies.[15]

To this end, π-conjugated small molecule perylene diimides (PDIs) have emerged as high performing CIL materials in OPV devices.[11,16] This is primarily due to their inherently high electron affinity and charge carrier mobilities arising from both the strongly electron withdrawing character of the dicarboxylic imide group and planar structure enabling tight intermolecular stacking. Additionally, they show excellent photostability arising from the large degree of π-conjugation which can stabilize radical anions. As well as the ease of chemical modifications which can further tune the work function modification of the cathode. For example, functionalizing PDI based materials with amino, or aliphatic amine groups at the imine position (*e.g.*, PDIN,[14] PDINN,[17] PDINN-F,[18] Fig. 1) has been shown to lead to self doping of the PDI core through the Lewis basic amine group.[19] While these self-doping type PDIs have shown excellent charge conductivity and CIL functionality, the solvent processing

Department of Chemistry, University of Calgary, 2500 University Drive N.W., Calgary, Alberta T2N 1N4, Canada. E-mail: gregory.welch@ucalgary.ca

† Electronic supplementary information (ESI) available: Experimental and synthetic details; MALDI-TOF MS; elemental analysis; NMR, and UV-vis spectroscopy data; cyclic and differential pulse voltammograms; OPV device testing data; and AFM data are included. See DOI: https://doi.org/10.1039/d3lf00166k

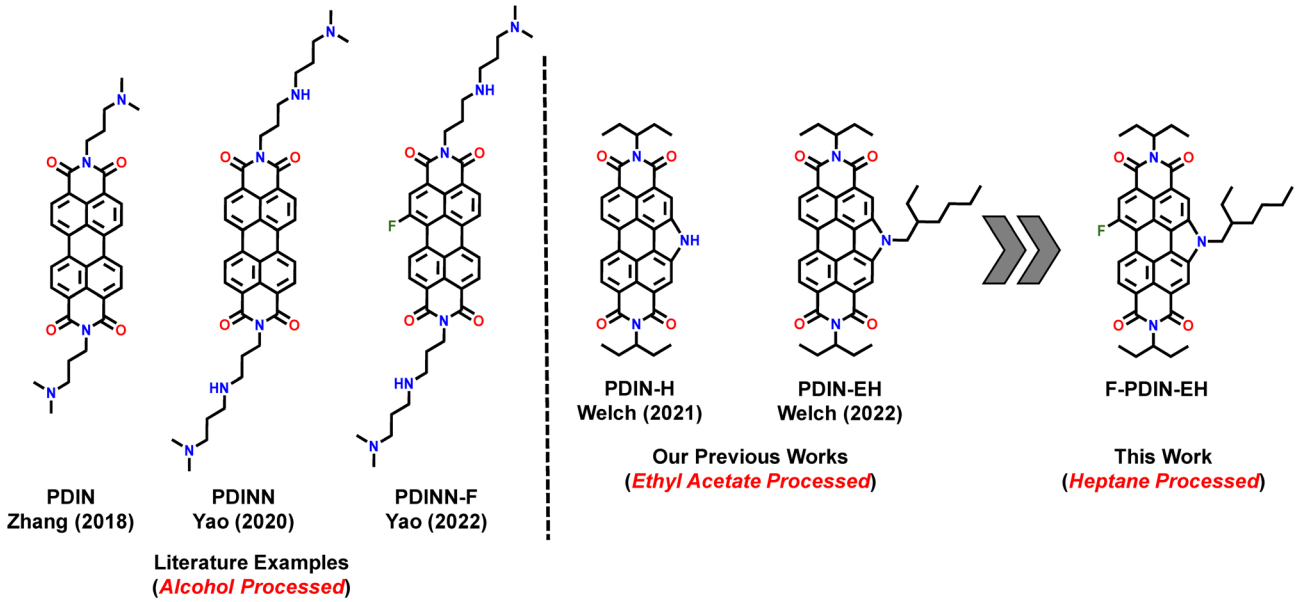

Fig. 1 Selected PDI derived materials used as cathode interlayers in conventional organic photovoltaic devices includes PDIN,[14] PDINN,[17] PDINN-F,[18] PDIN-H,[20] and PDIN-EH[21,22] towards the design of the new F-PDIN-EH material.

window is limited to highly polar solvents such as methanol (MeOH).[14,17,18] A survey of the literature processing conditions of high performing CILs reveals that alcohols, *e.g.*, MeOH, ethanol (EtOH), or trifluoroethanol (TFE), are exclusively used as the processing solvents for 55 previously reported CIL materials outside of our group (Table S1†). In our view the reason for using alcohols is compatibility with the photoactive layer in that the alcohol does not dissolve the organic photoactive film.

As OPV technology moves towards commercialization, sustainable and scalable manufacturing is important and necessitates the employment of green solvents to process the functional organic layers. While MeOH and EtOH, commonly used for CIL processing, can be considered green solvents under the composite sustainability score (G),[23] this limits the types of materials used for CIL layers to ones with polar functional groups and thus can decrease compatibility with BHJ layers which are typically hydrophobic. Additionally, the effective employment of commercially scalable R2R (*e.g.*, slot-die) coating processes in OPV manufacturing requires the use of processing solvents which evaporate on a slower timescale than methanol (T_b: 64.7 °C, G = 5.8) so to prevent the precipitation of material in the tubing or print heads to obtain an ideal smooth, uniform film.[24]

We have previously reported the compound PDIN-EH, a PDI derived CIL material soluble in ethanol (T_b: 78.4 °C, G = 6.6) and ethyl acetate (T_b: 77.1 °C, G = 6.7) for conventional OPVs which resulted in some of the highest device metrics for all slot-die coated OPVs made under ambient conditions.[21,22] In an effort to further expand the solvent processing window of CIL materials, herein, we report on a new fluorinated CIL, F-PDIN-EH for improved green solvent solubility. F-PDIN-EH can be processed from both polar solvents (butanol, T_b: 117.7 °C, G = 6.7; ethyl acetate) and non-polar solvents (heptane, T_b: 98.4 °C, G = 5.6) to deliver OPV devices (PM6:Y6 based) with PCEs > 10%, similar to our previous near record numbers. To the best of our knowledge, this is the first report of a material processed from heptane for use in OPVs and opens the door for both use of different materials and processes for CIL in OPVs.

Synthesis and optoelectronic characterization

The compound F-PDIN-EH was synthesized in one step through a halogen exchange of Br-PDIN-EH with KF (Fig. 2a, see ESI† for complete details). Structure and purity were confirmed using MALDI-TOF mass spectrometry, ^{1}H, ^{13}C, and ^{19}F NMR spectroscopies (Fig. S1 and S3–S5†). and CHN elemental analysis (Fig. S2†). Cyclic voltammetry was used to determine the redox properties with two reversible reductions occurring at −1.33 V and −1.59 V and a single reversible oxidation occurring at +1.06 V, (referenced to the Fc/Fc^{+} redox couple). Using the $E_{1/2}$ potentials the HOMO and LUMO energy levels were estimated to be −5.9 and −3.5 eV, respectively, comparable to all other N-annulated PDI compounds.[25]

Optical properties of F-PDIN-EH were probed using UV-visible absorption and photoluminescence spectroscopies in both solution and as thin-films (Fig. 2c and S6 and S7b†). In solution, F-PDIN-EH exhibits a signature PDI profile with the 0–0, 0–1, and 0–2 transitions at 525 nm, 489 nm, and 461 nm, respectively. Transitioning to the film shows a broadened profile with the 0–1 transition at 489 nm dominant. F-PDIN-EH has an emission λ_{max} at 535 nm (Fig. S6†) in solution and 575 nm in the film (Fig. S7b†).

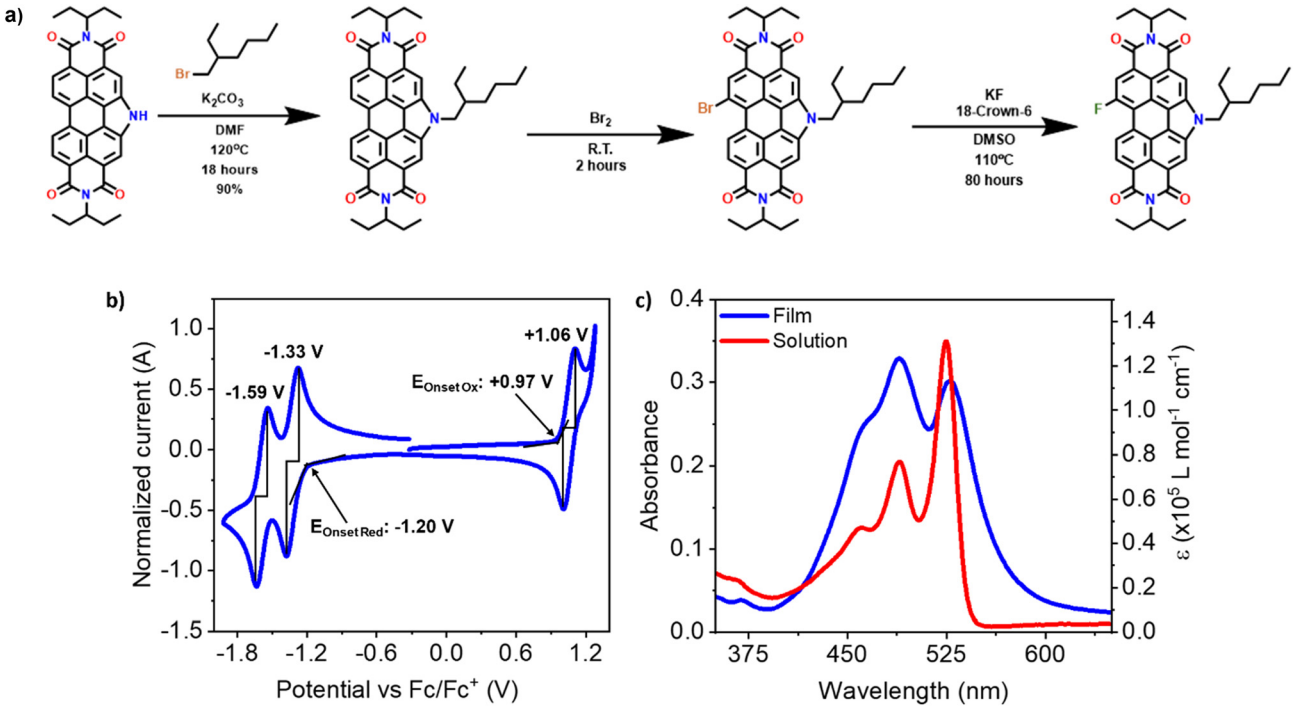

Fig. 2 (a) The synthetic route to F-PDIN-EH. (b) Cyclic voltammogram of F-PDIN-EH, measured in CH_2Cl_2 under N_2 with 0.1 M $TBAPF_6$ supporting electrolyte in dichloromethane solution at 100 mV s^{-1}. Internal reference to ferrocene/ferrocenium redox couple. $E_{1/2}$ values listed along with the onset of both oxidation and reduction. Lines show the anodic and cathodic peaks used to determine $E_{1/2}$ (WE = glassy carbon, CE = Pt-wire, pseudo RE = Ag/AgCl). (c) The solution optical absorption spectra of F-PDIN-EH in $CHCl_3$ (~10^{-5} M) and thin film optical absorption spectra of F-PDIN-EH film spin cast from chloroform (10 mg mL^{-1}, 1500 rpm).

Solubility and processing

It is a well known phenomena from pharmaceutical chemistry that aromatic fluorine substitution improves the bioavailability of medicinal compounds, which can be understood as increasing the compounds affinity for solubilizing in organic solvents.[26] Critical to this study is the processing of the F-PDIN-EH into uniform thin-films suitable for use as CILs. The solvents heptane, ethyl acetate, and butanol were selected as they are considered green, have varied polarities, and relatively lower vapor pressures which are good for maintaining ink consistency during the slot-die coating process. To assess the impact of fluorination on the processability of CIL materials for slot-die coated devices, the room temperature maximum solubility of the F-PDIN-EH was measured in the selected solvents (see ESI†). The maximum solubility of F-PDIN-EH was 1.8 mg mL^{-1} in heptane, 10.0 mg mL^{-1} in ethyl acetate, and 0.6 mg mL^{-1} in butanol. Comparing to non-fluorinated PDIN-EH, these values correspond to an improvement in solubility of 9.2-fold for

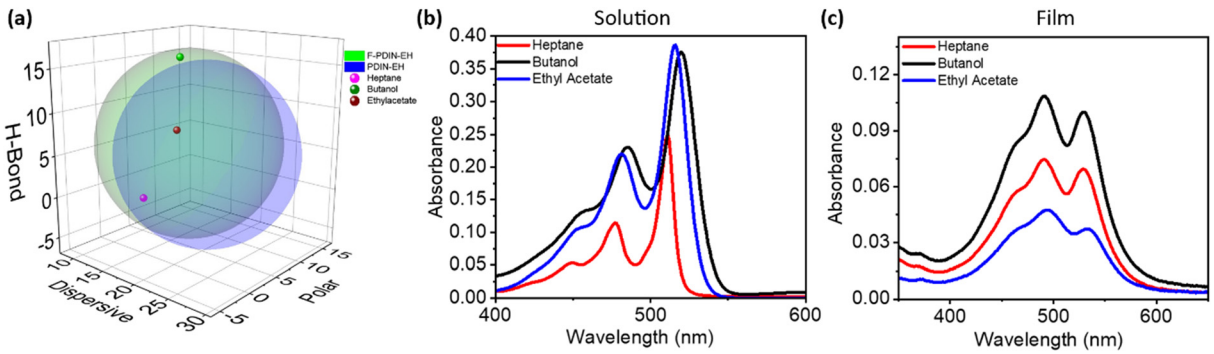

Fig. 3 (a) The Hansen solubility spheres of F-PDIN-EH and PDIN-EH inset with heptane, butanol, and ethyl acetate HSPs. (b) Solution UV-visible absorption spectra of F-PDIN-EH in heptane, butanol, and ethyl acetate taken in a 10 mm pathlength quartz cuvette (~10^{-5} M). (c) Thin film UV-visible absorption of F-PDIN-EH spin cast from heptane (2 mg mL^{-1}, 1000 rpm), ethyl acetate (2 mg mL^{-1}, 1000 rpm), and butanol (2 mg mL^{-1}, 3000 rpm).

heptane, 1.8-fold for ethyl acetate, and 1.3-fold for butanol (Table S2†). The largest increase in solubility for heptane is attributed to the increased lipophilic character of the fluorinated aromatic.[26,27]

To help further explain the changes in solubility the Hansen solubility parameters (HSPs) for both F-PDIN-EH and PDIN-EH were determined and plotted (Fig. 3a). These parameters allow one to quantitatively predict the miscibility of a solute with a given solvent by simple comparison of the HSP values, where the more similar the solute HSPs to a solvent or solvent mixture's HSPs the more miscible the two should be.[28] To determine the HSPs, 32 solvents were assessed for their ability to solubilize either F-PDIN-EH or PDIN-EH (Table S3†). For determination of the HSPs the solvent must be classified as "good" or "bad" in its ability to solubilize the material in question.[28,29] For this work, "good" was defined as >0.5 mg mL^{-1} solubility while "bad" was defined as <0.5 mg mL^{-1} solubility as it is common to cast very thin films from dilute solutions of CIL materials in OPV device stacks. From this, it was found that F-PDIN-EH has a greater emphasis on hydrogen bonding type interactions in dissolution while PDIN-EH has a greater emphasis on polarity type interactions in dissolution.

There have been very few studies exploring the underlying reasons aromatic fluorination improves solubility and these primarily focus on the induced changes in aggregation and crystalline structure after fluorination.[30–33] When a hydrogen atom is replaced by fluorine, a dipole moment is induced across the molecular surface with a large amount of electron density inductively localized around the fluorine atom.[31] This perturbation of electron density within the aromatic core commonly results in anti-parallel stacking arrangements where the region of high electron density around the fluorine interacts with the region of low electron density on another part of the molecule through C–H—F interactions.[30,32,33] These are shown to have a high degree of similarity to those interactions typically seen in weak hydrogen bonding systems, *i.e.* C–H—O or C–H—N, and are suggested to be correlated to the more soluble nature of fluorinated aromatics.[30,32] The calculated HSPs in this work align well with these findings, where F-PDIN-EH is more reliant on the hydrogen bonding parameter than is PDIN-EH. Additionally, unlike the other halogen atoms, *i.e.*, chlorine, bromine, and iodine, fluorine is very small and unpolarizable which results in a lack of induced dipole interactions typically seen in desolvation in polar media such as water, resulting in a region of polar hydrophobicity, and an increase in solubility in organic solvents.[31] It is therefore suggested that the increase in solubility seen in fluorinated aromatic compounds compared to their non-fluorinated counterparts should be seen as primarily arising from changes to the crystalline packing arrangement of the molecules, the emergence of a hydrophobic region on the molecule due to the non-polarizable nature of fluorine atoms, and to the heightened importance of hydrogen bonding found in C–H—F interactions.

Looking to the UV-visible spectroscopies, in solution, F-PDIN-EH displays a slight degree of positive solvatochromic character where the absorption profiles are red-shifted according to polarity typical for N-annulated PDI materials, owing to the reduced influence from non-polar solvents on excited states (Fig. 3b).[22] Notably, in films, casting from any of the tested solvents results in a near identical optical profile for both materials, indicating no significant impact of solvent choice on F-PDIN-EH film formation (Fig. 3c and S8d†).

Processing solvent interactions with PM6:Y6 BHJ

In order to evaluate any possible solvent–BHJ interactions, blank solvents (heptane, ethyl acetate, and butanol) were

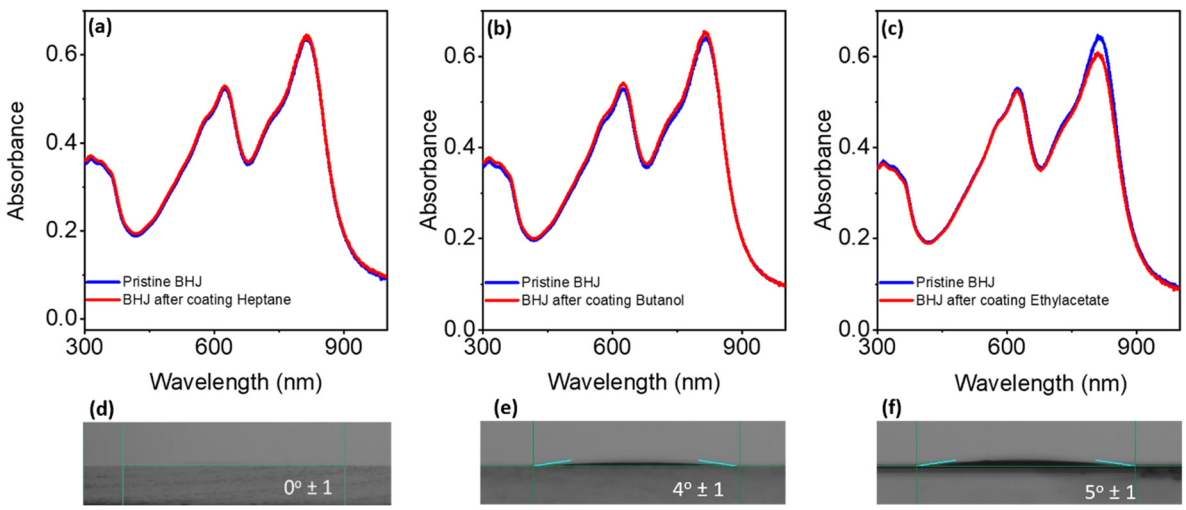

Fig. 4 The optical absorption spectra of the PM6:Y6 BHJ films before (blue) and after (red) slot-die coating (a) heptane, (b) butanol, and (c) ethyl acetate atop BHJ films. The contact angle measurements of d) heptane e) butanol, and f) ethyl acetate drops upon the BHJ.

Table 1 OPV device figures of merit for spin and slot-die coated F-PDIN-EH as cathode interlayers. Statistics were determined from the average of fifteen devices

CIL	CIL coating method	Processing solvent	V_{OC} (V)	J_{SC} (mA cm^{-2})	FF (%)	PCE$_{avg}$ (%)
No	—	—	0.69 ± 0.01	23.81 ± 0.38	49.64 ± 1.41	8.21 ± 0.25
F-PDIN-EH	Spin	Ethyl acetate	0.81 ± 0.01	24.01 ± 0.49	53.15 ± 0.35	10.34 ± 0.14
		Butanol	0.80 ± 0.005	23.96 ± 0.30	54.73 ± 1.26	10.60 ± 0.33
		Heptane	0.80 ± 0.002	24.36 ± 0.27	54.93 ± 0.73	10.61 ± 0.19
	Slot-die		0.79 ± 0.003	24.59 ± 0.72	51.34 ± 0.59	10.01 ± 0.21

applied *via* slot-die coating on top of PM6:Y6 BHJ films. Structures of PM6 and Y6 are showing in Fig. S18.† The optical absorption spectra were taken before and after the application of the processing solvent (Fig. 4). The application of ethyl acetate to the BHJ film caused a ~6% decrease in BHJ absorption intensity at 815 nm (Fig. 4b). This area corresponds to the peak absorption (λ_{max}) of NFA (Y6). The absorption spectra of the original Y6 films before and after being exposed to ethyl acetate displayed similar patterns (Fig. S19†). This loss was attributed to the partial dissolution of Y6 by ethyl acetate, as previously reported.[21] Notably, the absorption spectra of BHJ films after being coated with heptane or butanol did not show any decrease in absorption intensity (Fig. 4a and b). This implies that the components of the BHJ were insoluble in heptane and butanol. Fig. S21† showcases Y6 (5 mg ml^{-1}) in all three solvents. As determined by the slight colouration of the solvent, Y6 appear to have a very low solubility in heptane as compared to ethyl acetate, while in butanol no noticeable solvation of Y6 is observed. In our view, heptane is a viable non-polar processing solvent for CIL deposition upon the PM6:Y6 BHJ as no noticeable decrease in absorption is observed without exposing the BHJ film to heptane far longer than is typical for R2R processed devices (Fig. S22†). Similar results were given when spin-coating rather than slot-die coating on top of either pristine Y6 (Fig. S19†) or the BHJ (Fig. S20†), however, spin-coating from heptane appears to have a slight impact on BHJ film absorption at 819 nm with no change in device performance compared to butanol (Table 1). Contact angle measurements were conducted to assess the wettability of the BHJ films with all three CIL processing solvents (Fig. 4d–f). Each of the three solvents exhibited contact angles in the 0–5° range. Heptane exhibited full wetting on the BHJ, indicating its suitability for CIL deposition through industry-standard R2R thin film coating techniques (*e.g.*, slot-die).

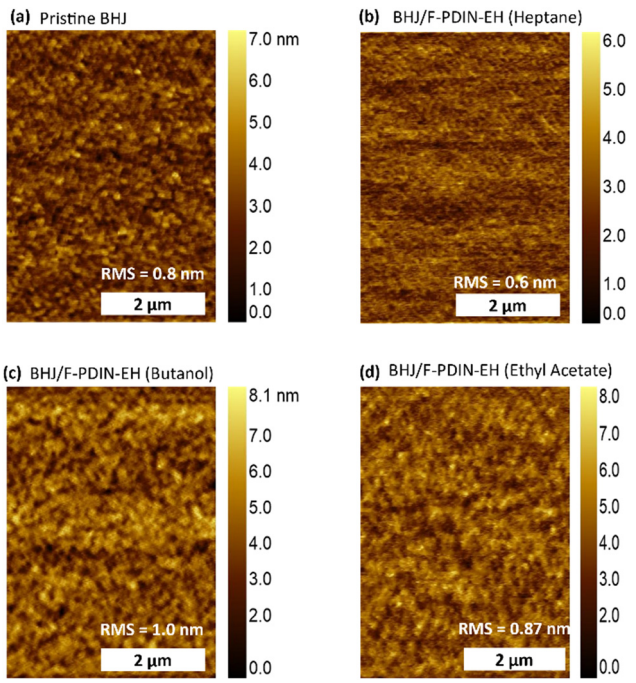

Fig. 5 Atomic force microscopy height images of (a) pristine PM6:Y6 BHJ and F-PDIN-EH atop the BHJ processed from (b) heptane, (c) butanol and (d) ethyl acetate.

Atomic force microscopy was used to analyze the BHJ surface before and after F-PDIN-EH was deposited *via* spin-coating from all three solvents. The root mean square (RMS) roughness of the pristine BHJ film was 0.8 nm, and it had a homogenous morphology (Fig. 5a). The F-PDIN-EH film that was processed with heptane (Fig. 5b) has a slightly lower RMS roughness of 0.6 nm, indicating the presence of a smooth film on top of the BHJ. While the butanol-processed film (Fig. 5c) had a higher RMS roughness of 1.0 nm, the film topography appears to be identical.

The ethyl acetate-processed CIL film (Fig. 5d) had a similar RMS roughness (0.87 nm) to that of the original BHJ. RMS roughness of the BHJ film after coating with blank heptane was also investigated (Fig. S23a†), appearing nearly identical (0.9 nm) to that of the pristine BHJ (Fig. 5a), and there was no discernible change in the texture. When slot-die-coated, the heptane-processed F-PDIN-EH film had the highest RMS roughness of 1.5 nm, with only a few visible aggregates (Fig. S23b†). This demonstrates that heptane is an effective solvent for depositing F-PDIN-EH *via* a scalable thin-film coating method (slot-die) to produce a uniform, smooth and continuous layer atop the BHJ surface.

Device characterization

A conventional OPV device architecture comprising of glass/ITO/PEDOT:PSS/BHJ/CIL/Ag was employed to assess the

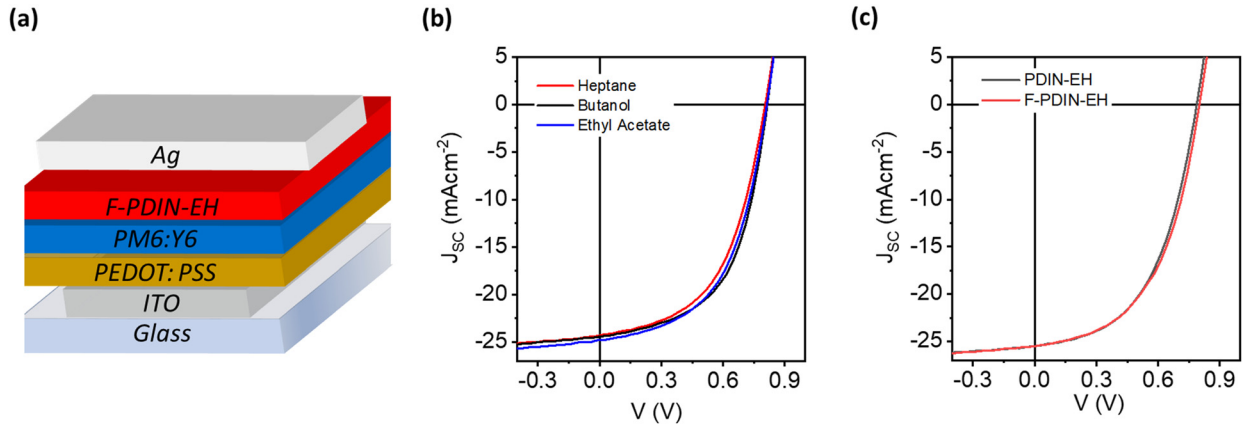

Fig. 6 (a) Representative conventional OPV device structure hosting F-PDIN-EH as CIL. (b) *J–V* curves of conventional OPV devices with F-PDIN-EH spin cast as a CIL. (c) Representative *J–V* curves of conventional OPV devices with F-PDIN-EH and PDIN-EH as CIL slot-die coated from heptane.

potential of F-PDIN-EH as a CIL (Fig. 6a), see the ESI† for full device fabrication details. All solution processing and thermal annealing steps were conducted under ambient conditions (T = 22 °C, RH = 40%). No post processing of the CIL thin films was carried out. F-PDIN-EH was spin-coated onto the photoactive layer in all three solvents at a concentration of 0.5 mg ml^{-1}. The scalability of the heptane-processable F-PDIN-EH was then demonstrated by depositing it *via* slot-die coating in an OPV. Representative *J–V* characteristics are presented in Fig. 6b. The control devices without any CIL were also characterized. The device figures of merit are summarized in Table 1.

Each device with F-PDIN-EH as CIL exhibited enhanced figures of merit with V_{OC}, J_{SC}, and FF values in the range 0.79–0.81 V, 23.82–24.59 mA cm^{-2} and 51.34–54.93%, respectively. In all cases, the average PCE was higher than 10%. Attributed to the aforementioned interaction with the BHJ, ethyl acetate processed CIL based devices showed slightly lower performance metrics. Heptane processed CIL based devices showed performance metrics on par with devices using butanol processed CIL. When deposited *via* industrially compatible slot-die coating, the heptane-processed F-PDIN-EH CIL yielded near identical figures of merit to the lab-scale spin coated devices (Table 1, Fig. 6).

Reference devices with PDIN-EH as CIL were also fabricated under identical processing conditions with a representative *J–V* curve shown in Fig. 6c. A comparison of the device metrics suggests that both N-annulated PDI CILs exhibited nearly identical performance. Typical for OPV devices fabricated in ambient conditions, significantly lower PCEs of ~11–13% were obtained as compared to the devices manufactured in a controlled environment (PCEs ~16%, N_2 filled glovebox, H_2O < 1 ppm, O_2 < 1 ppm).[34,35] All of the reference device metrics obtained in this study are comparable to those from our prior study, with slight discrepancies attributed to variations between device batches due to laboratory humidity conditions.[21,22]

Conclusion

In this work, we have reported on a new fluorinated N-annulated perylene diimide and utilized the compound as a cathode interlayer in green solvent processed organic photovoltaics. The new compound F-PDIN-EH exhibited increased solubility in a series of green solvents of differing polarity (butanol, ethyl acetate, and heptane) compared to the non-fluorinated derivatives. Notably a 10-fold increase in heptane solubility was found. Heptane was also demonstrated for the first time to be a useful solvent for the formation of cathode interlayers, not washing away the underlying BHJ films and fully weeting the surface. Air-processed OPVs using a PM6:Y6 BHJ and with the F-PDIN-EH as the were successfully fabricated using both spin coating and slot-die coating methods using butanol, ethyl acetate, or heptane as the interlayer processing solvent. When compared to devices cast without an interlayer, all device figures of merit improved with the when using F-PDIN-EH as a CIL regardless of processing solvent, resulting in an increase of the PCE from around 8.2% to 10.6% (all air-processed devices). The results indicate fluorination of small molecule cathode interlayer materials is a viable strategy for enhancing the processability window, especially in the case of non-polar processing solvents such as heptane, with maintained device performance.

Conflicts of interest

There are no conflicts to declare.

Acknowledgements

We acknowledge funding from the NSERC DG program (2019-04392), the Canada Foundation for Innovation, and the University of Calgary. This research was undertaken thanks in part to funding from the Canada First Research Excellence Fund (CFREF).

References

1 P. G. V. Sampaio, M. O. A. González, P. de Oliveira Ferreira, P. da Cunha Jácome Vidal, J. P. P. Pereira, H. R. Ferreira and P. C. Oprime, *Int. J. Energy Res.*, 2020, **44**, 9912–9931.
2 Y. Cui, L. Hong and J. Hou, *ACS Appl. Mater. Interfaces*, 2020, **12**, 38815–38828.
3 G. Zhang, F. R. Lin, F. Qi, T. Heumüller, A. Distler, H.-J. Egelhaaf, N. Li, P. C. Y. Chow, C. J. Brabec, A. K.-Y. Jen and H.-L. Yip, *Chem. Rev.*, 2022, **122**, 14180–14274.
4 G. Yu, J. Gao, J. C. Hummelen, F. Wudl and A. J. Heeger, *Science*, 1995, **270**, 1789–1791.
5 Q. Guo, Q. Guo, Y. Geng, A. Tang, M. Zhang, M. Du, X. Sun and E. Zhou, *Mater. Chem. Front.*, 2021, **5**, 3257–3280.
6 D. Meng, R. Zheng, Y. Zhao, E. Zhang, L. Dou and Y. Yang, *Adv. Mater.*, 2022, **34**, 2107330.
7 Y. Cui, Y. Xu, H. Yao, P. Bi, L. Hong, J. Zhang, Y. Zu, T. Zhang, J. Qin, J. Ren, Z. Chen, C. He, X. Hao, Z. Wei and J. Hou, *Adv. Mater.*, 2021, **33**, 2102420.
8 N. Ahmad, H. Zhou, P. Fan and G. Liang, *EcoMat*, 2022, **4**, e12156.
9 J. H. Kang, J. H. Lee, B. Walker, J. H. Seo and G. S. Chang, *J. Appl. Phys.*, 2022, **132**, 050701.
10 H. Tang, Y. Bai, H. Zhao, X. Qin, Z. Hu, C. Zhou, F. Huang and Y. Cao, *Adv. Mater.*, 2023, 2212236.
11 J. Yao, Q. Chen, C. Zhang, Z.-G. Zhang and Y. Li, *SusMat*, 2022, **2**, 243–263.
12 S. Dong, Z. Hu, K. Zhang, Q. Yin, X. Jiang, F. Huang and Y. Cao, *Adv. Mater.*, 2017, **29**, 1701507.
13 D. Di Carlo Rasi, P. M. J. G. van Thiel, H. Bin, K. H. Hendriks, G. H. L. Heintges, M. M. Wienk, T. Becker, Y. Li, T. Riedl and R. A. J. Janssen, *Sol. RRL*, 2019, **3**, 1800366.
14 Z.-G. Zhang, B. Qi, Z. Jin, D. Chi, Z. Qi, Y. Li and J. Wang, *Energy Environ. Sci.*, 2014, **7**, 1966–1973.
15 R. Sorrentino, E. Kozma, S. Luzzati and R. Po, *Energy Environ. Sci.*, 2021, **14**, 180–223.
16 M. Zhang, Y. Bai, C. Sun, L. Xue, H. Wang and Z.-G. Zhang, *Sci. China: Chem.*, 2022, **65**, 462–485.
17 J. Yao, B. Qiu, Z.-G. Zhang, L. Xue, R. Wang, C. Zhang, S. Chen, Q. Zhou, C. Sun, C. Yang, M. Xiao, L. Meng and Y. Li, *Nat. Commun.*, 2020, **11**, 2726.
18 J. Yao, S. Ding, R. Zhang, Y. Bai, Q. Zhou, L. Meng, E. Solano, J. A. Steele, M. B. J. Roeffaers, F. Gao, Z.-G. Zhang and Y. Li, *Adv. Mater.*, 2022, **34**, 2203690.
19 B. Russ, M. J. Robb, B. C. Popere, E. E. Perry, C.-K. Mai, S. L. Fronk, S. N. Patel, T. E. Mates, G. C. Bazan, J. J. Urban, M. L. Chabinyc, C. J. Hawker and R. A. Segalman, *Chem. Sci.*, 2016, **7**, 1914–1919.
20 E. Cieplechowicz, R. Munir, M. A. Anderson, E. L. Ratcliff and G. C. Welch, *ACS Appl. Mater. Interfaces*, 2021, **13**, 49096–49103.
21 A. Hoff, M. Martell, A. Gasonoo, J. D. B. Koenig, P. Simón Marqués, E. Cieplechowicz, M. Pahlevani and G. C. Welch, *Adv. Eng. Mater.*, 2023, **25**, 2201437.
22 A. Hoff, A. Gasonoo, M. Pahlevani and G. C. Welch, *Sol. RRL*, 2022, **6**, 2200691.
23 C. Larsen, P. Lundberg, S. Tang, J. Ràfols-Ribé, A. Sandström, E. Mattias Lindh, J. Wang and L. Edman, *Nat. Commun.*, 2021, **12**, 4510.
24 A. C, D. K. Dubey, M. Pahlevani and G. C. Welch, *Adv. Mater. Technol.*, 2021, **6**, 2100264.
25 M. E. Farahat and G. C. Welch, *Colorants*, 2023, **2**, 151–178.
26 S. DiMagno and H. Sun, *Curr. Top. Med. Chem.*, 2006, **6**, 1473–1482.
27 B. E. Smart, *J. Fluorine Chem.*, 2001, **109**, 3–11.
28 M. Díaz de los Ríos and E. Hernández Ramos, *SN Appl. Sci.*, 2020, **2**, 676.
29 D. T. Duong, B. Walker, J. Lin, C. Kim, J. Love, B. Purushothaman, J. E. Anthony and T.-Q. Nguyen, *J. Polym. Sci., Part B: Polym. Phys.*, 2012, **50**, 1405–1413.
30 V. R. Thalladi, H.-C. Weiss, D. Bläser, R. Boese, A. Nangia and G. R. Desiraju, *J. Am. Chem. Soc.*, 1998, **120**, 8702–8710.
31 J. C. Biffinger, H. W. Kim and S. G. DiMagno, *ChemBioChem*, 2004, **5**, 622–627.
32 K. Fuchibe, T. Morikawa, K. Shigeno, T. Fujita and J. Ichikawa, *Org. Lett.*, 2015, **17**, 1126–1129.
33 K. Fuchibe, K. Shigeno, N. Zhao, H. Aihara, R. Akisaka, T. Morikawa, T. Fujita, K. Yamakawa, T. Shimada and J. Ichikawa, *J. Fluorine Chem.*, 2017, **203**, 173–184.
34 H. Liu, D. Yuan, H. Jiang, S. Li, L. Zhang and J. Chen, *Energy Environ. Sci.*, 2023, **16**, 3474–3485.
35 A. Maeda, R. Liu, K. Yu, S. Lee, K. Nakano, M. Takakuwa, S. Zhang, K. Tajima, K. Fukuda, S. Umezu and T. Someya, *J. Phys. Mater.*, 2021, **4**, 044016.